Full Paper

Journal of the Brazilian Chemical Society

https://dx.doi.org/10.21577/0103-5053.20250162

J. Braz. Chem. Soc. **2025**, *36*, 12, e-20250162, 1-9

Surface-Enhanced Raman Scattering-Based Adsorption Isotherm of 4-Mercaptobenzoic Acid in Chitosan-Protected Gold Nanoparticles

Patrícia L. de Oliveira,[a,b] *Patrícia B. Santos,*[a] *Giovana A. Pimentel,*[a] *Débora G. de Oliveira*[a,c] *and Gustavo F. S. Andrade*[*,a]

[a]*Departamento de Química, Instituto de Ciências Exatas, Universidade Federal de Juiz de Fora, 36036-330 Juiz de Fora-MG, Brazil*

[b]*Departamento de Áreas Acadêmicas, Instituto Federal de Goiás, Campus Itumbiara, 75524-010 Itumbiara-GO, Brazil*

[c]*Departamento de Ciências Exatas e da Terra, Universidade do Estado de Minas Gerais, Unidade Ubá, 36500-000 Ubá-MG, Brazil*

4-Mercaptobenzoic acid (4-MBA) adsorption behavior was studied through an adsorption isotherm with surface-enhanced Raman scattering as the spectroscopic probe molecule, using chitosan-protected gold nanoparticles (AuNP). As the surface coverage was lower, 4-MBA molecules were reoriented, which led to the carboxylate group interaction with AuNP, besides the thiolate interaction, based on experimental and density-functional theory-based results. The adsorption process was fitted considering Langmuir isotherms, and a Gibbs energy of adsorption of –25 kJ mol^{-1} was obtained.

Keywords: 4-mercaptobenzoic acid, gold nanoparticle, adsorption isotherm, surface-enhanced Raman spectroscopy, chitosan

Introduction

Molecular adsorption onto a nanostructured plasmonic metal may result in the surface-enhanced Raman scattering (SERS), provided a suitable exciting radiation is used.[1] Compared to normal Raman scattering, the most striking advantage of SERS is the consequent spectrum signal intensification. Two mechanisms may have been used to explain the SERS effect: electromagnetic and chemical.[2] The electromagnetic model is related to the local field enhancement caused by the excitation of the surface electrons of plasmonic nanostructures caused by the interaction between the correct frequency incident radiation and the metallic nanostructure. The excitation leads to a coherent oscillation of the metallic surface electrons, which is known as the localized surface plasmon resonance (LSPR). This excitation causes a local electric field enhancement and a consequent Raman signal increase; it is highly accepted that plasmonic effects are responsible for most of the SERS enhancement.[3-5] The chemical effect is related to a charge transfer between the metal and the molecule, associated to a new electronic state that allows the resonance of incident radiation, resulting in the enhancement of the Raman scattering of the bands associated with modes affected by the charge transfer.[6,7]

The SERS effect has been used in various fields of nanoscience, such as photocatalysis, electrochemistry, and chemical and biosensing.[8-11] Among the advantages of SERS, the information richness related to the vibrational nature of the effect is notable.[10,11] The amount of information in a SERS spectrum allows, for instance, to consider specific surface selection rules[12] to infer molecular orientation on the plasmonic nanostructured surfaces.[13-15]

One key feature of the SERS effect is that the interaction between nanoparticles, forming the so-called hot spots, is essential for obtaining high-performance Raman scattering enhancement. Although crucial for high performance,[16] this feature poses challenges to the use of SERS as an analytical tool because small changes in the aggregation of nanostructures, which may be caused by changes in the adsorbate concentration among other species, result in substantial changes in the hot spot structure, leading

*e-mail: gustavo.andrade@ufjf.br
Editor handled this article: Izaura C. N. Diógenes (Executive)

to significant variations in SERS intensities.[17] Despite the structural obstacle, the efforts to carefully tailor SERS substrates and find suitable surface modifications have been shown to take SERS to become a potentially reliable analytical technique.[18]

The possibility of obtaining SERS-based adsorption isotherms relies on maintaining the aggregation state of nanoparticles over a wide range of adsorbate concentrations; the change in aggregation state will strongly influence the SERS intensity. To avoid aggregation, the use of nanoparticles protected by an appropriate modifier is essential; for example, it has been shown possible to study the adsorption isotherms of polycyclic aromatic hydrocarbons in lucigenin modified Ag nanoparticles,[19] and organochloride pesticides in dithiol functionalized Ag nanoparticles.[20] It has been proposed that chitosan is a suitable modifier for gold nanoparticles,[21,22] and allowed obtaining adsorption constants for dyes such as crystal violet and IR-820,[23] as well as developing chitosan-protected hot-spots.[24]

4-Mercaptobenzoic acid (4-MBA), structure presented in Figure 1, has been utilized as a SERS reporter molecule in many studies,[25-29] due to several favorable characteristics of this substance. The most striking characteristic is the possibility of using 4-MBA as a nanometric pH sensor, as the SERS spectra present characteristic changes with pH; additionally, the molecule adsorbs chemically to Ag and Au nanoparticles, resulting in a stable platform that may be inserted in samples as small as biological cell organelles.[30] It is well-known that the thiol group of 4-MBA has a high affinity with gold surfaces, forming stable self-assembled monolayers by the bonding formation between thiol and Au surface.[31] In addition, the carboxylic group may also act as a relevant adsorption site in some conditions.[32,33] It has been proposed that the adsorption on Ag nanostructures can occur by both the thiolate and the COO^- group for pH ≥ 7, or solely by the thiolate group for pH < 7.[32-34] For Au nanostructures, previous reports[34,35] suggest that adsorption occurs solely by the dissociated thiol group. The SERS spectral range between 900 and 1800 cm^{-1} is widely used for 4-MBA because it has the most intense bands and a well-known band assignment.[34,35] Two bands are commonly monitored for this molecule, because of their strong signal: 1076 cm^{-1} (ring breathing) and 1590 cm^{-1} (CC ring stretching).

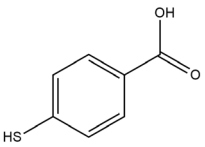

Figure 1. Structure of 4-mercaptobenzoic acid.

Considering the discussion above, this study presents experimental and theoretical results of 4-MBA interacting with chitosan-protected gold nanoparticles (AuNP) and a SERS-based adsorption isotherm. Langmuir and Frumkin models were used to fit experimental data to obtain thermodynamic data and discuss the adsorption process.

Experimental

Materials

Tetrachloroauric(III) acid trihydrate ($HAuCl_4$) (99%), 4-MBA (99%), trisodium citrate dihydrate, and chitosan medium molecular weight (deacetylation degree 75-87%) were purchased from Sigma-Aldrich. Sodium hydroxide p.a. micro pearls (99%) and glacial acetic acid p.a. were obtained from Synth and Vetec Química Fina (Brazil), respectively. Deionized water (Millipore Synergy-UV, resistivity 18.2 MΩ cm) was used in all experiments.

Apparatus

Raman and SERS experiments were performed at a confocal Raman microscope model SENTERRA (Bruker) coupled with an Olympus BX51 microscope. Experimental parameters were: 632.8 nm wavelength excitation, 20 mW laser power, 50× objective (numerical aperture (NA) = 0.50), 30 s accumulation time for solid 4-MBA Raman spectrum, 200 s for 4-MBA in solution, and 100 s accumulation time for colloidal suspensions containing 4-MBA for SERS spectra. UV-Vis spectra of the colloidal samples were obtained with an Ocean Optics USB2000 equipment with a 1 nm resolution and 1 mm optical path.

Synthesis of gold nanoparticles

Gold nanoparticles were prepared by adapting an earlier reported procedure.[36] Firstly, a seed solution was prepared by heating an aqueous solution of sodium citrate trihydrate (90 mL, 2.2 mmol L^{-1}), under vigorous stirring, until the solution boiled. Then, an aqueous solution of $HAuCl_4$ (600 µL, 25 mmol L^{-1}) was added, and the stirring was continued for 10 min. After this, the three-neck flask containing seed solution was transferred to an ultra-thermostatic water bath previously heated and maintained at 90 °C. The growth solution was initiated when the seeds reached 90 °C, followed by the addition of 600 µL of sodium citrate solution (60 mmol L^{-1}), and 2 min later, 600 µL of $HAuCl_4$ (25 mmol L^{-1}). This procedure was repeated 13 times every 30 min. To avoid solvent evaporation, a condenser was used in all steps.

The scanning electron microscopy results indicated that the obtained AuNPs presented a low dispersion in size, with an average diameter of 55 nm, as may be observed in Figure S1 (Supplementary Information section).

Sample preparation

The solubility of 4-MBA is low in water, so the solution was prepared using a NaOH aqueous solution (0.15 mol L^{-1}) because in alkaline media, the solubility of the compound increases considerably due to the ionization of the carboxylic group. Therefore, an alkaline solution of 4-MBA at 1 mmol L^{-1} was prepared and used as a stock solution for SERS sample dilution.

An acetic acid aqueous solution (1% v/v) was prepared for chitosan solubilization. Thus, a stock solution containing 10 g L^{-1} of chitosan was maintained under stirring for 24 h, ensuring a complete solubilization.

To prepare SERS samples, a 1:1 (v/v) mixture of colloidal suspension and 4-MBA solution was always used to avoid any local over-concentration.[37] To prepare the chitosan-protected AuNP suspension, a procedure similar to previously reported[23] was used: the chitosan concentration of the stock solution was adjusted to allow adding a constant volume to the colloidal suspension to avoid dilution effects in the SERS intensity. Samples were prepared according to the following sequence: firstly, 500 µL AuNP + 100 µL chitosan (10 g L^{-1}) + 30 min under vortex; secondly, 100 µL 4-MBA (x mol L^{-1}) + 300 µL deionized water + 15 min under vortex, where x is the concentration of the stock solution prepared to achieve three different order of magnitude levels. 4-MBA final concentrations were 10^{-4}, 10^{-5}, and 10^{-6} mol L^{-1}, ranging from 1.0 to 3.0 (with 0.5 increments) for each level. The resulting pH was 4.7 for the SERS samples. All samples and data acquisition were obtained at an ambient temperature of 21 °C.

The SERS spectra were acquired by excitation of the colloidal solution contained in a plastic container (ca. 300 µL) and directly excited in the regular back-scattering configuration of the Raman spectrometer.

Density-functional theory calculations

The structures of the model complexes (Figure 2) were optimized based on the density-functional theory (DFT) as implemented in the Gaussian 09 (Revision D.01) suite of programs.[38] The B3LYP functional[39,40] was used in all calculations, and a 6-31G(d)[25] basis set was used for all atoms except the metal; a cluster containing 10 gold atoms (Au) was computed considering the pseudo-potential LANL2DZ basis set.[41,42] An implicit dielectric medium was simulated considering the IEFPCM and water as the solvent.[43] It is worth mentioning that the chosen setup was based on the description capability of the model at a relatively low computational cost. The calculated vibrational frequencies were corrected by a linear correction factor of 0.9613, as indicated by Wong[44] for the 6-31G(d) basis set. The calculated Raman activities were corrected by finite temperature and exciting radiation (considering λ_0 = 632.8 nm).[45] The reported calculated spectra present the above corrections in the spectral plot.

Results and Discussion

Raman and surface-enhanced Raman scattering of 4-mercaptobenzoic acid

Figure 2 presents model complex structures optimized using the DFT calculations detailed above, showing the interaction of 4-MBA with a ten-atom gold cluster in a continuous dielectric water medium. The charges were selected according to the deprotonation of the carboxyl group. Differences between complexes in Figures 2b and 2c were the position of 4-MBA before the structural optimization. The C-structure (Figure 2c) was optimized with the carboxylate group positioned closer to the surface compared to structure B (Figure 2b). The XYZ-coordinates of the optimized structures may be found in "XYZ-Coordinates for the optimized structures for A, B, and C complexes" section of the Supplementary Information file.

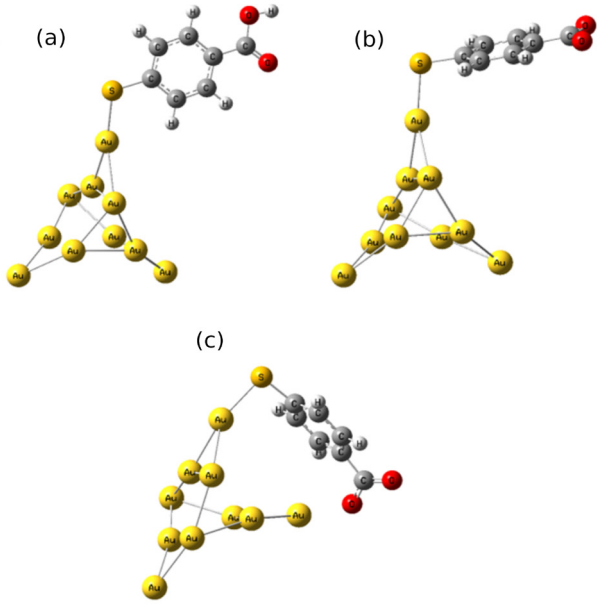

Figure 2. 4-Mercaptobenzoic acid interaction with gold cluster after theoretical calculations. (a) Doublet, 0 charge, complex A; (b,c) doublet, –1 charge, complexes B and C, respectively.

Structures presented in Figure 2 were used to calculate the vibrational modes given in Table 1 (A-C) and the Raman theoretical spectra.

The normal Raman spectra of 4-MBA in both solid and in aqueous alkaline solution ([4-MBA] = 1.0×10^{-3} mol L^{-1}) are shown in Figure 3, while SERS and theoretical Raman spectra for the model complex Ag_{10}(4-MBA) are shown in Figure 4. Selected bands from the Raman spectra in the figures are marked, and their vibrational mode assignments can be seen in Table 1 (for the weak bands, consult Figure S2, Supplementary Information).

Firstly, in the Raman spectrum of solid 4-MBA a weak band at 910 cm^{-1} may be observed, which is associated with SH in-plane bending, which is observed solely in the normal Raman spectrum of Figure 3. The characteristic band of the ν(S–H) at 2567 cm^{-1} was also observed (Figure S3, Supplementary Information section); neither of the bands were observed in Raman spectrum of 4-MBA in solution, which is due to the low intensity of the Raman bands in the analyzed concentration. Both bands tend to vanish in SERS because the sulfur atom of thiophenols has a high affinity for nanostructured gold surfaces, forming a strong chemical bond at the cost of releasing the H atom of the thiol group.[31] That was observed in the SERS results presented in Figure 4,

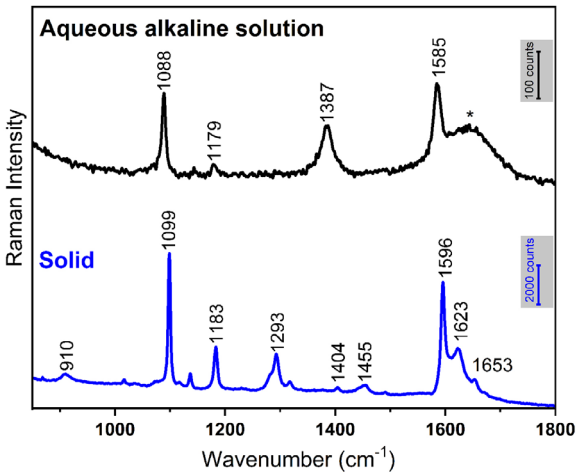

Figure 3. Normal Raman spectrum of 4-MBA solid and in alkaline solution. [4-MBA] in solution = 1.0 mmol L^{-1}. *Water.

as both the band at 900 and 2567 cm^{-1} (not shown) vanished; therefore, there is evidence that the interaction between sulfur and gold nanoparticles was always present in the experimental results obtained in our study. In the theoretical calculations performed for all model complexes the S atom of the 4-MBA molecule was considered in the thiolate form.

The SERS bands related to the ring breathing (1076 cm^{-1}) and CC symmetric stretching (1589 cm^{-1})

Table 1. Theoretical (A, B, and C) and experimental (D and F) vibrational modes assignments for 4-mercaptobenzoic acid surface-enhanced Raman scattering and normal Raman

Theoretical			Experimental				Assignment
A	B	C	D[a]	F[b]	Solid	Solution[c]	
–	–	–	–	–	910		δ(SH)
954	–	940	998	989	1016		γ(CH)
989	988	989	1013	1017	1072		$\delta(CCC)_{ring}$ trigonal
1051	1046	1051	1076	1074	1099	1088	ring breathing
1074	–	–	1112	–	1118		δ(CH) + ν(C–OH)
–	1093	1108	–	1118	–		δ(CH) + $\nu(C–COO^-)$
1145	–	–	1135	–	1136		δ(CH) + δ(OH)
1179	1145	1154	1179	1172	1183	1179	δ(CH)
1273	1257	1265	–	1256	1280		$\nu(CC)_{ring}$ (Kekulé)
1294	–	1272	–	1291	1293		δ(CH)
–	1277	1287	1272	–	–		$\nu(CC)_{ring}$ + δ(CH)
–	1329	–	–	1346	–	1387	$\nu(C–COO^-)$ + $\delta(COO^-)$
1336	–	–	–	–	1404		δ(C–O–H)
1389	1367	1372	1394	1383	1455		$\nu(CC)_{ring}$ + δ(CH)
1471	1454	1463	1482	1477	1490		δ(CH)
1534	1530	1532	–	1537	–		$\nu(CC)_{ring}$
1575	1566	1571	1589	1582	1596	1585	$\nu_s(CC)_{ring}$
–	1633	1613	1650	1640	–		$\nu_{as}(COO^-)$
1708	–	–	1700	–	–		ν(C=O)

4-MBA concentration: [a]300 μmol L^{-1} (SERS), [b]3 μmol L^{-1} (SERS); [c]1 mmol L^{-1} (Raman). ν: stretching; δ: in-plane bending; γ: out-of-plane bending.

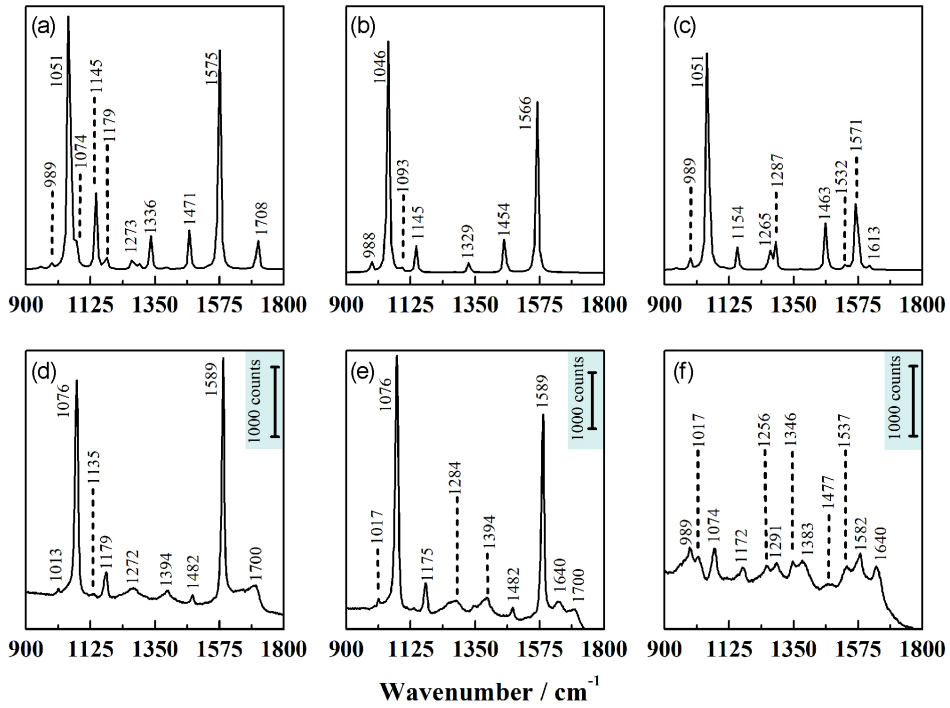

Figure 4. (a-c) Theoretical Raman spectra of the Ag_{10}(4-MBA) complexes and (d-f) experimental SERS spectra of 4-mercaptobenzoic acid, where (d), (e), and (f) correspond to molecular concentration at 300, 30, and 3 μmol L^{-1}, respectively.

modes will be further discussed here, because they are the most intense and well-resolved bands, even at low concentrations, and also the most discussed in the literature.[34,35] A blue shift is observed for the band at 1589 cm^{-1}, which the increase in deprotonated molecules can explain; however, the band at 1076 cm^{-1} exhibits no significant shifts (Figures 4d-4f).[34] Another SERS bands worth mentioning are the band at 1346 cm^{-1} and the spectral range between 1640-1700 cm^{-1}. The band at 1346 cm^{-1}, which may be assigned to the symmetric COO^- stretching of the carboxylate group of deprotonated 4-MBA, was detected only for low concentrations, indicating that the predominant species on surface is the protonated 4-MBA for higher concentrations. Still, for 3 μmol L^{-1}, there is deprotonated 4-MBA adsorbed as well.

The SERS bands observed in the spectral range at about 1640-1700 cm^{-1} also reveal the molecular interaction behavior between 4-MBA oxygen atoms and the gold surface. The band at 1700 cm^{-1}, assigned to ν(C=O),[35] characteristic of the protonated species, was observed only at higher concentrations. As the concentration decreased, a band at 1650 cm^{-1} was detected, which can be attributed to the anti-symmetrical stretching of the carboxylate group.[34] However, as the concentrations decreased, this band shifted to lower wavenumbers, which corroborates the hypothesis that at low concentrations, molecular reorientation occurs, allowing 4-MBA to start interacting with the surface through the carboxylate group. Although the band shifts are evidence of interaction of the carboxylate group with the gold surface, it should also be noticed that the relative intensities of the SERS bands of 4-MBA change as concentration decreases; the most relevant changes are related to the decrease in relative intensities of the 1074 and 1582 cm^{-1} (values observed in the spectra at 3 μmol L^{-1}), which are the most intense bands assigned to in-plane vibrational modes of the adsorbate. Decreasing their intensities is a crucial indication that a molecular reorientation has occurred.[12] However, a detailed discussion of the reorientation may be difficult because at the lower concentrations some bands may be associated to citrate, the capping agent for the AuNPs: the bands at 1017, 1256, 1346, 1383 and 1582 cm^{-1} fall in regions that raise the possibility of coming from citrate.[46,47] It is worth mention that citrate has already been shown to interfere in the spectra of adsorbates in low surface coverage over citrate-caped AuNPs.[47,48]

The above discussions allow to infer that, as the 4-MBA concentration decrease, molecular reorientation occurs, leading to an additional interaction with AuNP through carboxyl group deprotonation, besides the thiolate bonding. Thus, the less covered surface would result in 4-MBA interacting, besides the S atom, via oxygen atoms by carboxyl group deprotonation. Nevertheless, it is worth mentioning that no specific band that could be direct evidence of the last interaction was found in the DFT results.

Figure 5 presents two schemes that summarize the SERS results: (Figure 5a) surface presenting high molecular coverage (high concentration) and (Figure 5b) the hypothesis of the molecular reorientation for low concentrations, where the carboxylate group starts to interact with the surface simultaneously with the sulfur atom.

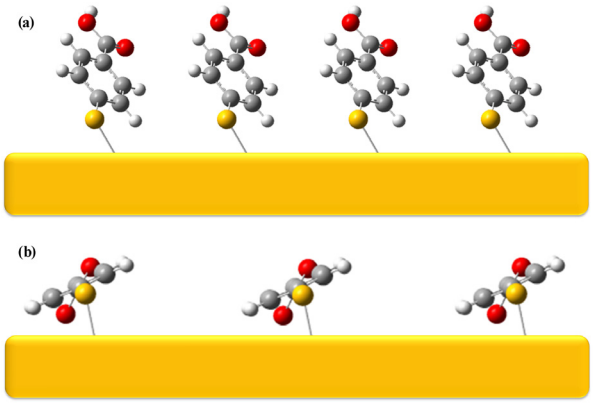

Figure 5. Self-assembled monolayer behavior suggested for 4-mercaptobenzoic acid at (a) high surface-coverage and (b) low surface-coverage.

Chitosan: surface-enhanced Raman scattering-based isotherms

The chitosan-protected AuNPs were relatively stable, and no uncontrolled aggregation was observable by adding 4-MBA, as one can see in the UV-Vis spectra (Figure S4, Supplementary Information). The adsorption behavior of 4-MBA on the surface of chitosan-protected AuNP was modelled using Langmuir adsorption isotherms.[49] The Langmuir model for the SERS context was adapted according to previous work described in the literature.[50] The equation used in the present study for the Langmuir adsorption isotherm model is presented in equation 1.

$$I_S = \frac{I_{MC}\, K_L\, [4MBA]}{1 + K_L\, [4MBA]} \quad (1)$$

where, I_s and I_{MC} are SERS intensity and SERS intensity at maximum coverage, respectively; K_L is the adsorption equilibrium constant and [4MBA] is the molar concentration of 4-mercaptobenzoic acid.

Equation 1 was used for plotting isotherm curves based on the SERS intensity as a function of concentration of 4-MBA.[23,24] To construct the isotherm curve, the I_s was measured as a relative intensity, considering the broad band of water at ca. 3410 cm^{-1} for all spectra data. The 4-MBA bands at 1076 and 1589 cm^{-1} were selected for this study due to their strong signals and sufficient separation from other bands, enabling precise intensity measurements. The relative intensity of the selected bands as a function of 4-MBA concentration and the Langmuir adsorption isotherm fitting are shown in Figure 6a. Table 2 shows the parameters extracted from the fitted curve, the maximum saturation intensity (I_{MC}) and the adsorption constant (K_L).

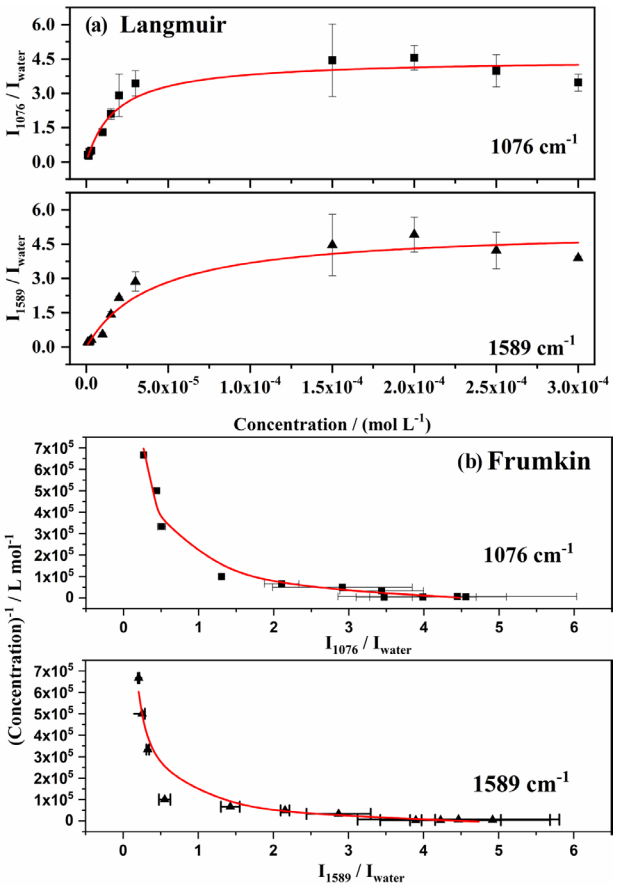

Figure 6. (a) Langmuir isotherm fitting for 4-MBA adsorbed in chitosan-protected AuNPs for the bands at 1076 and 1589 cm^{-1}; (b) Frumkin isotherm fitting for the same bands as in (a). Red lines represent the fitting, while black squares represent the experimental data. The 4-MBA band intensity was measured relative to the water band at 3410 cm^{-1}.

It may be observed in Table 2 a reasonably good fitting correlation with the experimental data, with values of R^2 (coefficient of determination) above 0.91, and the calculated K_L values have the same order of magnitude for both bands considered. Furthermore, the maximum relative intensity was similar to the limit of the fitting uncertainty, and the concentration of the self-assembled monolayer formation showed the same order of magnitude at about 10^{-4} mol L^{-1}. The observation of a reasonable fit of the SERS intensity of 4-MBA bands with the Langmuir model indicates that chitosan is an efficient protecting layer for the study of adsorption phenomena using SERS.

However, it is relevant to discuss the assumptions of the Langmuir model for adsorption isotherms, which

Table 2. Langmuir and Frumkin isotherm models fitted parameters for 4-mercaptobenzoic acid adsorption in chitosan-protected gold nanoparticles and Gibbs free energy

Parameter	SERS band / cm^{-1}	
	1076	1589
Langmuir model		
K_L	$5.53 \times 10^4 \pm 1.00 \times 10^4$	$2.42 \times 10^4 \pm 0.56 \times 10^4$
I_{MC}	4.51 ± 0.31	5.20 ± 0.50
R^2	0.96814	0.91951
$\Delta G°_{ads}$[a] / (kJ mol^{-1})	−26.7 ± 0.18	−24.7 ± 0.23
Frumkin model		
K_L	$4.17 \times 10^4 \pm 0.95 \times 10^4$	$2.80 \times 10^4 \pm 1.13 \times 10^4$
I_{MC}	4.55 ± 1.13	4.51 ± 1.77
w	−921	−921
R^2	0.97599	0.95748
$\Delta G°_{ads}$[a] / (kJ mol^{-1})	−26.0 ± 5.9	−25.0 ± 10.1

[a]$\Delta G°_{ads}$ was obtained considering the equation $\Delta G°_{ads} = -RT \ln K_L$ for T = 294.15 K. SERS: surface-enhanced Raman scattering; K_L: adsorption equilibrium constant; I_{MC}: intensity at maximum coverage; R^2: coefficient of determination; $\Delta G°_{ads}$: Gibbs energy of adsorption; w: interaction parameter.

consider that every adsorption sites are identical, and the lateral interaction of the adsorbing layer is negligible.[51] The AuNPs surface used in the present study had citrate and chitosan as surface stabilizers, which may result in several different adsorption sites over the gold surface. Considering the possibility of a distribution of different adsorption sites, the Langmuir model may not be the best choice for describing the adsorption process of 4-MBA on the AuNPs surface. Among the different adsorption isotherm models, the Frumkin model may be useful to improve the description of the adsorption site upon considering the lateral interactions in the adsorbing layer.[51] The equation for the Frumkin isotherm is given in equation 2.[52]

$$[4MBA] = \frac{I_S}{K_L (I_{MC} - I_S)} \exp\left(w \frac{I_S}{I_{MC}}\right) \quad (2)$$

where w is an interaction parameter.

The fitting curves based on the Frumkin model are presented in Figure 6b, and the fitted parameters are presented in Table 2. One may observe in Figure 6b that a good fit was obtained, which is verified by the values of R^2, which are larger than 0.95 for both 1076 and 1589 cm^{-1} bands. It may also be observed that the fitted values for both K_L and I_{MC} were close to those obtained in the fitting based on the Langmuir model, when one considers the uncertainty in both fitted curves. The improvement in the fitting based on the Frumkin model indicates that lateral interactions are relevant for the adsorption of 4-MBA on the chitosan modified AuNPs.

The differences observed in the K_L parameter value, which are in the limit of the uncertainty for both values, may be related to the fact that the band at 1589 cm^{-1} presents significant blue shifts with concentration, when compared to the 1076 cm^{-1} band. The blue shift can be associated with the molecular deprotonation of the 4-MBA adsorption process, which is spontaneous in neutral medium. Regardless of the observed change in the adsorption constant, from the data in Table 2, we may infer that the 4-MBA adsorption process is spontaneous, presenting a $\Delta G°_{ads}$ (Gibbs energy of adsorption) around −25 kJ mol^{-1}.

Conclusions

Summarizing, the adsorption process of 4-MBA on chitosan-protected AuNP was studied using SERS, due to the surface protective effect of chitosan, which avoided uncontrolled aggregation in the presence of the adsorbate. The process was measured as favorable and spontaneous, as expected from a thiophenol on a gold nanostructured surface, with a value of approximately −25 kJ mol^{-1}, which agrees with previous measurements for the adsorption of thiols on gold.[53,54]

There could also be stated that molecular reorientation may occur as the concentration of the molecule is reduced, as well as deprotonation of the carboxyl group, which the interaction between the oxygen atoms and the surface can explain. The change in orientation may be responsible for the slight difference in the fitted parameters for the SERS results comparing two different bands, such as the K_L values. The present study reinforces the potential of using chitosan as a protective agent for gold nanoparticles for applications in the estimation of adsorption parameters based on SERS, widening the application of this plasmon-based spectroscopic technique.

Supplementary Information

Supplementary Information file (XYZ coordinates for DFT complex model, scanning electron micrograph of the AuNPs, surface-enhanced Raman spectra emphasizing weak bands, high-wavenumber region of the Raman spectra of 4-MBA solid and in solution and UV-Vis spectra of the AuNPs modified by citrate, chitosan and 4-MBA is available free of charge at http://jbcs.sbq.org.br as PDF file.

Data Availability Statement

The data will be available from the authors upon a reasonable request.

Acknowledgments

The authors thank FAPEMIG (CEX-APQ-00340-22), CNPq, and CAPES (financing code 001) for financial support. P. L. O. and D. G. O. thank CAPES for fellowships. G. A. P. thanks UFJF for a fellowship.

Author Contributions

P.L.O.: data curation, formal analysis, investigation, validation, visualization, writing original draft; P.B.S.: data curation, formal analysis, software, writing - review and editing; G.A.P.: formal analysis, investigation, visualization, writing - review and editing; D.G.O.: conceptualization, formal analysis, investigation, writing - review and editing; G.F.S.A.: conceptualization, data curation, formal analysis, funding acquisition, project administration, resources, validation, writing - review and editing.

References

1. Aroca, R.; *Surface-Enhanced Vibrational Spectroscopy*; John Wiley & Sons: Hoboken, USA, 2007.
2. Le Ru, E. C.; Etchegoin, P. G.; *Principles of Surface-Enhanced Raman Spectroscopy*; Elsevier B. V.: Amsterdam, Netherlands, 2009.
3. Ding, S.-Y.; You, E.-M.; Tian, Z.-Q.; Moskovits, M.; *Chem. Soc. Rev.* **2017**, *46*, 4042. [Crossref]
4. Grasseschi, D.; dos Santos, D. P.; *Quim. Nova* **2020**, *43*, 1482. [Crossref]
5. dos Santos, D. P.; Grasseschi, D.; *Quim. Nova* **2020**, *43*, 1463. [Crossref]
6. Otto, A.; *J. Raman Spectrosc.* **2005**, *36*, 497. [Crossref]
7. Chaudhry, I.; Hu, G.; Ye, H.; Jensen, L.; *ACS Nano* **2024**, *18*, 20835. [Crossref]
8. Langer, J.; Jimenez de Aberasturi, D.; Aizpurua, J.; Alvarez-Puebla, R. A.; Auguié, B.; Baumberg, J. J.; Bazan, G. C.; Bell, S. E. J.; Boisen, A.; Brolo, A. G.; Choo, J.; Cialla-May, D.; Deckert, V.; Fabris, L.; Faulds, K.; García de Abajo, F. J.; Goodacre, R.; Graham, D.; Haes, A. J.; Haynes, C. L.; Huck, C.; Itoh, T.; Käll, M.; Kneipp, J.; Kotov, N. A.; Kuang, H.; Le Ru, E. C.; Lee, H. K.; Li, J.-F.; Ling, X. Y.; Maier, S. A.; Mayerhöfer, T.; Moskovits, M.; Murakoshi, K.; Nam, J.-M.; Nie, S.; Ozaki, Y.; Pastoriza-Santos, I.; Perez-Juste, J.; Popp, J.; Pucci, A.; Reich, S.; Ren, B.; Schatz, G. C.; Shegai, T.; Schlücker, S.; Tay, L.-L.; Thomas, K. G.; Tian, Z.-Q.; Van Duyne, R. P.; Vo-Dinh, T.; Wang, Y.; Willets, K. A.; Xu, C.; Xu, H.; Xu, Y.; Yamamoto, Y. S.; Zhao, B.; Liz-Marzán, L. M.; *ACS Nano* **2020**, *14*, 28. [Crossref]
9. Bantz, K. C.; Meyer, A. F.; Wittenberg, N. J.; Im, H.; Kurtuluş, Ö.; Lee, S. H.; Lindquist, N. C.; Oh, S.-H.; Haynes, C. L.; *Phys. Chem. Chem. Phys.* **2011**, *13*, 11551. [Crossref]
10. Fan, M.; Andrade, G. F. S.; Brolo, A. G.; *Anal. Chim. Acta* **2020**, *1097*, 1. [Crossref]
11. Fan, M.; Andrade, G. F. S.; Brolo, A. G.; *Anal. Chim. Acta* **2011**, *693*, 7. [Crossref]
12. Moskovits, M.; *J. Chem. Phys.* **1982**, *77*, 4408. [Crossref]
13. Pessanha, P. V. A.; Sant'Ana, A. C.; *J. Braz. Chem. Soc.* **2025**, *36*, e-20250121. [Crossref]
14. de Oliveira, R.; Sant'Ana, A. C.; *J. Braz. Chem. Soc.* **2023**, *34*, 1309. [Crossref]
15. da Silva, B. N.; Bessa, L. A. M.; Marques, F. C.; Andrade, G. F. S.; Lourenço Junior, V.; Mizubuti, E. S. G.; Tronto, J.; Izumi, C. M. S.; *Vib. Spectrosc.* **2023**, *129*, 103606. [Crossref]
16. Moskovits, M.; *J. Raman Spectrosc.* **2005**, *36*, 485. [Crossref]
17. Le Ru, E. C.; Etchegoin, P. G.; Meyer, M.; *J. Chem. Phys.* **2006**, *125*, 204701. [Crossref]
18. Fan, M.; Brolo, A. G.; *ACS Nano* **2025**, *19*, 3969. [Crossref]
19. López-Tocón, I.; Otero, J. C.; Arenas, J. F.; Garcia-Ramos, J. V.; Sanchez-Cortes, S.; *Anal. Chem.* **2011**, *83*, 2518. [Crossref]
20. Kubackova, J.; Fabriciova, G.; Miskovsky, P.; Jancura, D.; Sanchez-Cortes, S.; *Anal. Chem.* **2015**, *87*, 663. [Crossref]
21. da Silva, H. B.; Peixoto, L. P. F.; Andrade, G. F. S.; *Plasmonics* **2025**, *20*, 7705. [Crossref]
22. Toledo, P. H. M.; Peixoto, L. P. F.; Fragneaud, B.; Andrade, G. F. S.; *J. Nanopart. Res.* **2024**, *26*, 74. [Crossref]
23. de Oliveira, D. G.; Peixoto, L. P. F.; Sánchez-Cortés, S.; Andrade, G. F. S.; *Vib. Spectrosc.* **2016**, *87*, 8. [Crossref]
24. de Oliveira, D. G.; Pimentel, G. A.; Andrade, G. F. S.; *Vib. Spectrosc.* **2020**, *110*, 103119. [Crossref]
25. Ji, X.; Xu, S.; Wang, L.; Liu, M.; Pan, K.; Yuan, H.; Ma, L.; Xu, W.; Li, J.; Bai, Y.; Li, T.; *Colloids Surf., A* **2005**, *257-258*, 171. [Crossref]
26. Luo, Z.; Li, W.; Lu, D.; Chen, K.; He, Q.; Han, H.; Zou, M.; *Microchim. Acta* **2013**, *180*, 1501. [Crossref]
27. Zeng, Y.; Pei, J.-J.; Wang, L.-H.; Shen, A.-G.; Hu, J.-M.; *Biosens. Bioelectron.* **2015**, *66*, 55. [Crossref]
28. Zhang, Y.; Zhang, H.; Li, D.; Naqvi, S. M. Z. A.; Abdulraheem, M. I.; Su, R.; Ahmed, S.; Hu, J.; *Spectrosc. Lett.* **2021**, *54*, 732. [Crossref]
29. Scarpitti, B. T.; Morrison, A. M.; Buyanova, M.; Schultz, Z. D.; *Appl. Spectrosc.* **2020**, *74*, 1423. [Crossref]
30. Kneipp, J.; Kneipp, H.; Wittig, B.; Kneipp, K.; *J. Phys. Chem. C* **2010**, *114*, 7421. [Crossref]
31. Vericat, C.; Vela, M. E.; Benitez, G.; Carro, P.; Salvarezza, R. C.; *Chem. Soc. Rev.* **2010**, *39*, 1805. [Crossref]
32. Michota, A.; Bukowska, J.; *J. Raman Spectrosc.* **2003**, *34*, 21. [Crossref]
33. Ho, C.-H.; Lee, S.; *Colloids Surf., A* **2015**, *474*, 29. [Crossref]
34. Liu, Y.; Yuan, H.; Fales, A. M.; Vo-Dinh, T.; *J. Raman Spectrosc.* **2013**, *44*, 980. [Crossref]
35. Gühlke, M.; Heiner, Z.; Kneipp, J.; *Phys. Chem. Chem. Phys.* **2015**, *17*, 26093. [Crossref]

36. Bastús, G. N.; Comenge, J.; Puntes, V.; *Langmuir* **2011**, *27*, 11098. [Crossref]
37. Darby, B. L.; Le Ru, E. C.; *J. Am. Chem. Soc.* **2014**, *136*, 10965. [Crossref]
38. Frisch, M. J.; Trucks, G. W.; Schlegel, H. B.; Scuseria, G. E.; Robb, M. A.; Cheeseman, J. R.; Scalmani, G.; Barone, V.; Petersson, G. A.; Nakatsuji, H.; Nakatsuji, H.; Li, X.; Caricato, M.; Marenich, A.; Bloino, J.; Janesko, B. G.; Gomperts, R.; Mennucci, B.; Hratchian, H. P.; Ortiz, J. V.; Izmaylov, A. F.; Sonnenberg, J. L.; Williams-Young, D.; Ding, F.; Lipparini, F.; Egidi, F.; Goings, J.; Peng, B.; Petrone, A.; Henderson, T.; Ranasinghe, D.; Zakrzewski, V. G.; Gao, J.; Rega, N.; Zheng, G.; Liang, W.; Hada, M.; Ehara, M.; Toyota, K.; Fukuda, R.; Hasegawa, J.; Ishida, M.; Nakajima, T.; Honda, Y.; Kitao, O.; Nakai, H.; Vreven, T.; Throssell, K.; Montgomery Jr., J. A.; Peralta, J. E.; Ogliaro, F.; Bearpark, M.; Heyd, J. J.; Brothers, E.; Kudin, K. N.; Staroverov, V. N.; Keith, T.; Kobayashi, R.; Normand, J.; Raghavachari, K.; Rendell, A.; Burant, J. C.; Iyengar, S. S.; Tomasi, J.; Cossi, M.; Millam, J. M.; Klene, M.; Adamo, C.; Cammi, R.; Ochterski, J. W.; Martin, R. L.; Morokuma, K.; Farkas, O.; Foresman, J. B.; Fox, D. J.; *Gaussian 09, Revision D.01*; Gaussian, Inc., USA, 2016.
39. Becke, A. D.; *Phys. Rev. A* **1988**, *38*, 3098. [Crossref]
40. Lee, C.; Yang, W.; Parr, G, R.; *Phys. Rev. B* **1988**, *37*, 785. [Crossref]
41. Hay, P. J.; Wadt, W. R.; *J. Chem. Phys.* **1985**, *82*, 270. [Crossref]
42. Wadt, W. R.; Hay, P. J.; *J. Chem. Phys.* **1985**, *82*, 284. [Crossref]
43. Tomasi, J.; Mennucci, B.; Cammi, R.; *Chem. Rev.* **2005**, *105*, 2999. [Crossref]
44. Wong, M. W.; *Chem. Phys. Lett.* **1996**, *256*, 391. [Crossref]
45. Zvereva, E. E.; Shagidullin, A. R.; Katsyuba, S. A.; *J. Phys. Chem. A* **2011**, *115*, 63. [Crossref]
46. Zhang, Y.; Wang, F.; Yin, H.; Hong, M.; *Adv. Nanopart.* **2013**, *2*, 104. [Crossref]
47. Vesga, M. J.; McKechnie, D.; Laing, S.; Kearns, H.; Faulds, K.; Johnston, K.; Sefcik, J.; *Colloids Surf., A* **2021**, *621*, 126523. [Crossref]
48. Oliveira, G. P.; Righi, A.; Almeida, M. R.; Andrade, G. F. S.; *Vib. Spectrosc.* **2023**, *129*, 103617. [Crossref]
49. Atkins, P.; de Paula, J.; *Physical Chemistry*, 8th ed.; W. H. Freeman: New York, USA, 2006.
50. Izquierdo-Lorenzo, I.; Sanchez-Cortes, S.; Garcia-Ramos, J. V.; *Anal. Methods* **2011**, *3*, 1540. [Crossref]
51. Urbina, P. A. M.; Berto, M.; Greco, P.; Sensi, M.; Borghi, S.; Borsari, M.; Bortolotti, C. A.; Biscarini, F.; *J. Mater. Chem. C* **2021**, *9*, 10965. [Crossref]
52. Chu, K. H.; Tan, B. C.; *Colloid Interface Sci. Commun.* **2021**, *45*, 100519. [Crossref]
53. Karpovich, D. S.; Blanchard, G. J.; *Langmuir* **1994**, *10*, 3315. [Crossref]
54. Paulo, T. D.; da Silva, M. A. S.; Pinheiro, S. D.; Meyer, E.; Pinheiro, L. S.; Freire, J. A.; Tanaka, A. A.; de Lima Neto, P.; Moreira, Í. S.; Diógenes, I. C. N.; *J. Braz. Chem. Soc.* **2008**, *19*, 711. [Crossref]

Submitted: August 6, 2025
Final version online: October 21, 2025